ICDM-3 special issues

INTERNATIONAL JOURNAL OF DAMAGE MECHANICS

International Journal of Damage Mechanics
0(0) 1–17

DOI: 10.1177/1056789519857121
journals.sagepub.com/home/ijd
SAGE

Localization of deformation and its effects on power-law singularity preceding catastrophic rupture in rocks

Jian Xue[1], Shengwang Hao[1,2], Rong Yang[1], Ping Wang[2] and Yilong Bai[1]

Abstract

Three distinct length scales are involved in the deformation evolution and catastrophic rupture of heterogeneous rocks in general: two essential ones are the specimen size macroscopically and the grain size at micro-scale respectively, the other is the emerging localized band of deformation and damage. The band initiates almost nearby the peak load, and the rupture eventually occurs afterwards within the localized band. In this paper, we report that with the evolution of concentrated high strain and damage in the localized band, a power-law singularity emerges within the localized band preceding the eventual rupture. The localization of deformation imposes a spatial non-uniqueness on the power-law singularity, and then leads to a trans-scale characteristic of the power-law singularity. Based on this characteristic, it is demonstrated that the singularity presented by the global response of a whole specimen comes from the singularity of local response in the localized band. The localization and the power-law singularity are associated precursory events, spatially and temporally, respectively, before macroscopic rupture. In particular, based on the power-law singularity exhibited in the zonal areas near or across the rupture surface, a prediction of the occurrence time of catastrophic rupture can be made accordingly. This provides a practically helpful approach to the prediction of rupture, merely by means of monitoring the zonal areas adjacent to the localized band.

Keywords

Localization, power-law singularity, trans-scale characteristic, catastrophic rupture, prediction

[1]State Key Laboratory of Nonlinear Mechanics (LNM), Institute of Mechanics, Chinese Academy of Sciences, Beijing, China
[2]School of Civil Engineering and Mechanics, Yanshan University, Qinhuangdao, China

Corresponding author:
Yilong Bai, State Key Laboratory of Nonlinear Mechanics (LNM), Institute of Mechanics, Chinese Academy of Sciences, Beijing, China.
Email: baiyl@lnm.imech.ac.cn

Introduction

Localization of deformation and damage is a general phenomenon in concrete (Jin et al., 2018; Li and Wu, 2018; Markeset and Hillerborg, 1995) and geological materials (Baud et al., 2004; Dewers et al., 2017; Harnett et al., 2018; Xu et al., 2004) and serves as an effective precursor of catastrophic rupture (Hao et al., 2007, 2010; Li et al., 2000). After localization, the strain field of a specimen bifurcates into a two-part continuum consisting of a less-deformation zone and a localized band where the deformation and damage are concentrated (Bai et al., 2001; Colpo et al., 2017; Hao et al., 2007, 2010; Hill and Hutchinson, 1975; Lockner et al., 1991; Rudnicki and Rice, 1975; Toussaint and Pride, 2002). The localized band then becomes mechanically and physically distinct from the outside zones. The rupture of a specimen eventually occurs in this localized band. As a consequence, the localized band with a smaller characteristic scale is a key inducing catastrophic rupture (Bai et al., 2001; Hao et al., 2007, 2010), which strongly depends on the nonlinear evolution and the rapid cascade of the micro-damages and micro-defects (Kale and Ostoja-Starzewski, 2017; Main et al., 2010; Rong et al., 2006; Wei et al., 2000).

Catastrophic rupture occurs when the energy release from the testing system and (or) the outside of the localized band compensates the requirement of the rupture energy of the localized band (Cook, 1965; Hao et al., 2007, 2010). It is a self-sustaining process that does not need any supplying of external work. In order to characterize the catastrophic rupture, Hao et al. (2013) and Xue et al. (2018) introduced a response function

$$R = d\Omega/d\lambda \tag{1}$$

defined as the relative change of response quantity Ω with respect to the controlling variable λ. At the rupture point, an infinitesimal increase of the controlling variable will lead to a finite increment of the response quantities (Hao et al., 2013). Thus, R is divergent at catastrophic rupture point and exhibits a singularity. More importantly, in the vicinity of the rupture point, R increases with a power-law acceleration with approaching to rupture point, that is

$$R = B_{\mathrm{F}}(1 - \lambda/\lambda_{\mathrm{F}})^{\beta_{\mathrm{F}}} \tag{2}$$

where B_{F} is a constant and β_{F} is the power-law singularity exponent. Subscript F represents the value at the rupture point. If the controlling variable λ increases linearly with respect to time, equation (2) can be rewritten as

$$d\Omega/dt = K(1 - t/t_{\mathrm{F}})^{\beta_{\mathrm{F}}} \tag{3}$$

where K is a constant and t_{F} is the rupture time. This expression (equation (3)) can also be deduced from the famous Voight's relation (Voight, 1988, 1989)

$$\ddot{\Omega}\dot{\Omega}^{-\alpha} = A \tag{4}$$

with $K = [A(\alpha - 1)]^{1/(1-\alpha)}$ and $\beta_{\mathrm{F}} = -1/(\alpha - 1)$. Here α is an exponent measuring the degree of non-linearity, and A is a constant. The dot represents the first and second derivatives of the response quantity Ω with respect to time. The validation of predicting rupture time based on equations (2) and (3) has been widely verified in many retrospective predictions (Boué et al., 2015; Hao et al., 2016; Smith and Kilburn, 2010; Voight and Cornelius, 1991; Xue et al., 2018) of laboratory experiments (Hao et al., 2013; Kilburn, 2012), landslides (Helmstetter et al., 2004), earthquakes (Ben-Zion and Lyakhovsky, 2002; Sornette and Sammis, 1995), and volcanic eruptions (Kilburn, 2003;

Main, 1999). Especially when $\beta_F = -1$ (i.e., $\alpha = 2$), the rupture time can be determined by extrapolating the inverse rate R^{-1} to the abscissa (Boué et al., 2015; Voight, 1988).

However, the power-law singularity exponent β_F is not always a constant in reported measurements but exhibits a large dispersion (Boué et al., 2015; Cornelius and Scott, 1993; Hao et al., 2017; Jin et al., 2012; Kilburn, 2003; Voight and Cornelius, 1991; Xue et al., 2018). The uncertainty resulting from the scatter of the exponent makes it difficult to use such methods for prediction of the rupture time (Boué et al., 2015; Hao et al., 2017; Xue et al., 2018). On the one hand, this change of the power-law exponent is inherently related to the energy criterion of catastrophic rupture (Xue et al., 2018). It has been shown that the power-law exponent β_F ranges from $-1/2$ to -1 (Xue et al., 2018). The closer to its lowest value -1 of β_F, the closer to the rupture process without work input the loading process becomes. On the other hand, this may also be related to the various data sets adopted from various stations corresponding to the concerned rupture event, for some of them are within or without the localized zone. As mentioned above, after localization, damage and deformation concentrate in the localized band and increase rapidly, and the eventual rupture occurs in this localized band. Hence, recognizing the relationship between localization and power-law acceleration precursor is essential for understanding catastrophic rupture and the scatter of the power-law exponent. Especially, the effects of localization on the power-law singularity with a changeable power-law exponent are crucial for the prediction of catastrophic rupture. This is particularly important in practice, because the data such as changes of length, tilt, acoustic emission and deformation, monitored in landslides, earthquakes and volcanic eruptions, are always measured in some local stations.

In this paper, the relationship between localization and power-law singularity has been investigated, based on the uniaxial compression tests of marbles. The spatio-temporal evolution of strain field on the specimen surface is measured by using the digital image correlation (DIC) method, and then the trans-scale behavior of the power-law singularity with a changeable power-law exponent is investigated by varying the size of sampling zone. Based on the power-law singularity of the responses near or across the rupture surface, a method is suggested to predict the lower and upper bounds of the rupture time in real-time. This method further implies a feasibility to predict the occurrence time of the natural catastrophic ruptures like earthquakes in terms of the data sets surveyed in local areas nearby the faults.

Experimental methodology

In experiments, rock (Marble) specimens are compressed by moving the crosshead of the testing machine at a speed of 0.05 mm/min. The governing displacement U of the testing machine, which is continuously measured by a linear variable differential transformer (LVDT) with a resolution of 1 μm, is the controlling variable. Specimens are cut into cubes with sizes of $20 \times 20 \times 40\,mm^3$ (Figure 1(a)) and loaded along the length direction by using MTS 810 material testing system with a stiffness about 210 kN/mm (Figure 1(b)). The average initial linear stiffness of specimens is 283 kN/mm.

The deformation u of a specimen along the length direction is measured by an extensometer held between the upper and lower platens (Figure 1(c)) with a resolution of 1 μm. The force sensor with a resolution 1 kN is mounted on the upper platen (Figure 1(b)). The DIC method (Hao et al., 2007; Xu et al., 2004) is used to acquire the displacement field and the strain field of a specimen surface (Figure 1(b)), and the speckle photos of the specimen surface are recorded with a rate of 25 frames per second by using a charge coupled device (CCD) with a resolution of 768 (H) × 576 (V). The loading and acquisition systems are shown in Figure 1(d).

Catastrophic rupture usually occurs beyond the peak load when the specimen is loaded by controlling the displacement (Figure 2). According to the energy criterion of catastrophic rupture,

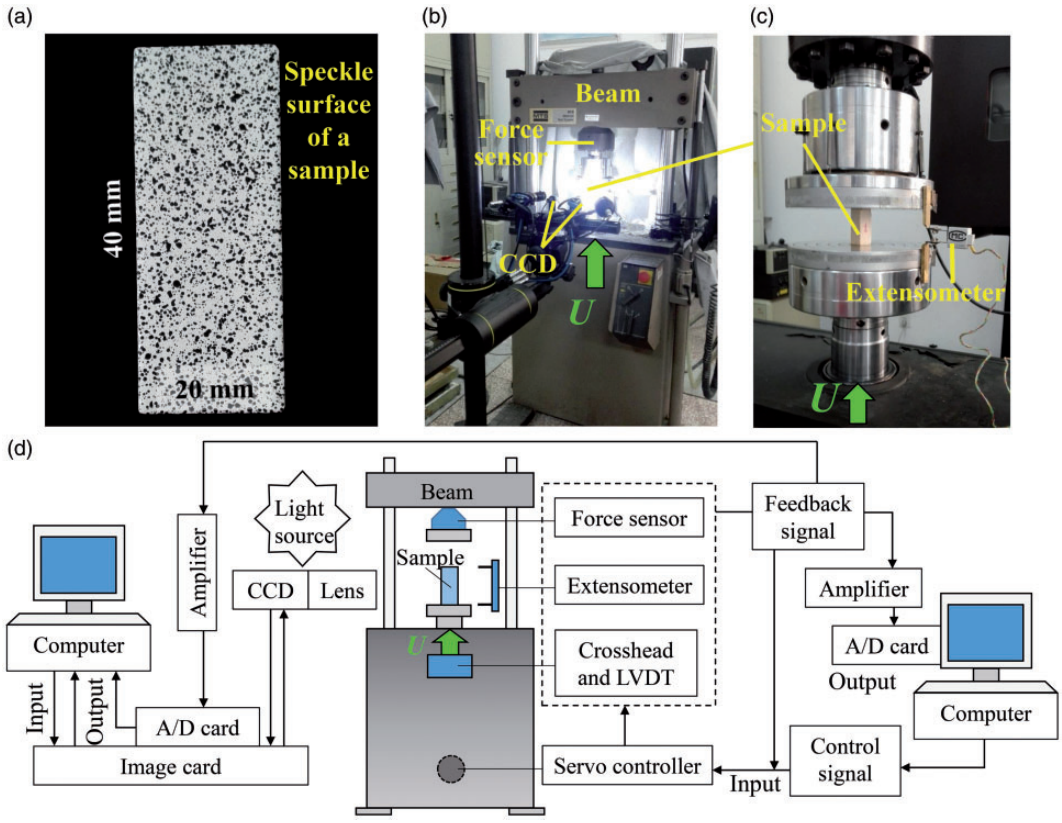

Figure 1. Illustrations of a tested specimen, the testing machine and the acquisition system. (a) A tested specimen with a speckle surface. (b) The MTS 810 testing system and the DIC acquisition system. (c) A close view of the platens, a tested specimen and the extensometer. (d) Schematic diagram of the testing and acquisition system.

the tangent slope of the F–u curve is equal to the negative stiffness (i.e., $-k$) of the testing machine at the rupture point (Figure 2; Cook, 1965; Salamon, 1970). It has been shown (Hao et al., 2013; Xue et al., 2018) that the response function $R = du/dU$, defined as the relative change of the global deformation u of a specimen with respect to the controlling displacement U, presents a power-law acceleration before rupture

$$R = B_{\mathrm{F}}(1 - U/U_{\mathrm{F}})^{\beta_{\mathrm{F}}} \tag{5}$$

When $U = U_{\mathrm{F}}$, R tends to infinite and exhibits a power-law singularity, which can be derived from the energy criterion (Xue et al., 2018).

Deformation localization and its spatiotemporal evolution

In order to illustrate the evolution properties of localization, a series of zonal areas parallel to the rupture surface (Figure 3(a)) of a specimen are meshed on the observed surface (Figure 3(b)).

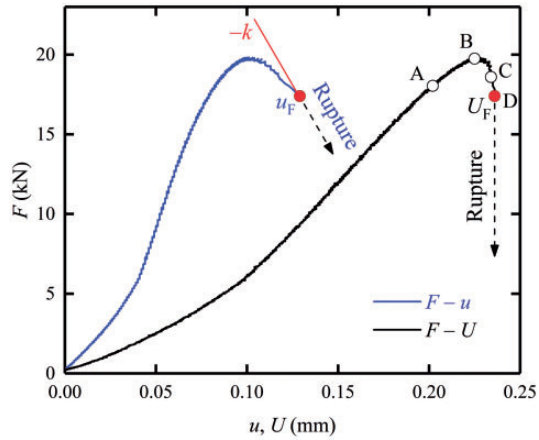

Figure 2. The typical force–displacement curve (F—U) and the force–deformation curve (F—u) of a specimen. Four points A, B, C, and D denote the representative states of the specimen at different loading stages. U_F and u_F represent the values of U and u at the catastrophic rupture. k represents the stiffness of the testing machine, and the red straight line with slope $-k$ is the tangent of F–u curve at the catastrophic rupture.

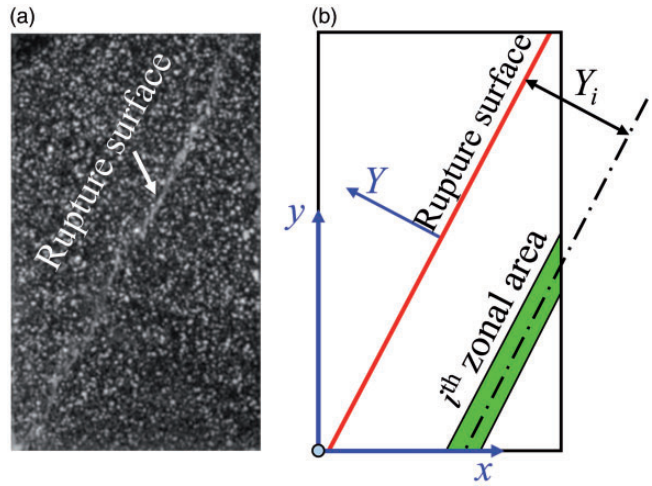

Figure 3. Rupture photo and the reference coordinate axes. (a) Eventual state of a specimen with a rupture surface. (b) The Cartesian coordinate systems on the observed surface of a ruptured specimen. The load is applied along y-direction, and Y-direction is perpendicular to the rupture surface. The narrow green zone parallel to the rupture surface illustrates one of the zonal areas.

A Cartesian coordinate system (xy-plane) is established on the observed surface, and the y-axis is parallel to the loading direction (Figure 3(b)). A reference axis of Y-direction is set to be perpendicular to the rupture surface, and then, as shown in Figure 3(b), Y_i denotes the distance between the center of the ith zonal area and the rupture surface. The width of one zonal area is far less than the characteristic length of a whole specimen, thus, these meshed zonal areas can be used to investigate the local evolution of the displacement filed and strain field on the observed surface of a specimen.

Figure 4 shows the displacement field (removed the global average values $\overline{\overline{u}}_x^*$ and $\overline{\overline{u}}_y^*$) on the observed surface of a specimen at four representative points of A, B, C, and D in Figure 2, where u_x^* and u_y^* represent the displacements in x- and y-directions, respectively. The upper symbol "=" denotes the average value of each displacement component of the whole specimen at every individual time. For example, $\overline{\overline{u}}_x^* = \frac{1}{M}\sum_{i=1}^{M} u_{xi}^*$, where M is the number of all calculation points on the whole observed surface. It can be seen that at the early elastic stage (e.g., at the point of A), the displacement field is almost uniform with small random fluctuations, and the contour lines are consistent with no distortion. Near the peak load point (subgraphs B in Figure 4), it begins to deviate from the uniform state and the contour lines become distorted. In some areas, the displacement gradients become large and then the deformation becomes concentrated, i.e., localization of deformation and damage begins to nucleate. The nucleation zone of the localization is located near the corners and the diagonal of a specimen surface (subgraphs B in Figure 4). After the peak load, the specimen enters the softening stage (Figure 2), and the sampling point C is located in such a stage. At this stage, the displacement contour lines of the surface are further distorted and become denser near the diagonal line. Both of the amplitude and gradient of the displacement increase rapidly. The localized band formed in this stage. Subgraphs D in Figure 4 are corresponding to the last photo captured before rupture. It can be seen that the rupture eventually occurs in the localized band (Figures 3(a) and 4).

Localization of damage and deformation is an essential characteristic preceding catastrophic rupture. Beyond the peak load, the bearing capacity of a specimen decreases rapidly (Figure 2) and the local displacement field changes drastically (Figure 5). In Figure 5, the average displacement components (i.e., $\bar{u}_x^*$ and $\bar{u}_y^*$) of all of the zonal areas present dramatically changes near the rupture point after removing the entire average values $\overline{\overline{u}}_x^*$ and $\overline{\overline{u}}_y^*$, and a large displacement gradient occurs between the positive growth region and the negative growth region. It is resulted from the trans-scale cascade of micro-damages and micro-defects, which destroys the uniformity of the field and leads to the emergence of localization (Rong et al., 2006).

The evolution of strain field (Figure 6) shows a more clear process of localization. As shown in Figure 6, $\bar{\varepsilon}_Y$ represents the strain component on the observed surface that is perpendicular to the rupture surface, and four subgraphs A, B, C, and D correspond to the representative states illustrated in Figure 2. It is seen that at the early elastic stage, the strain field is almost uniform (Figure 6-A) with small random fluctuations, then the localized band nucleates (Figure 6-B) and extends (Figure 6-C), finally the extension of the localized band leads to a catastrophic rupture (Figure 6-D).

Response function and power-law singularity in zonal area

The localized band shown in Figure 6 is very narrow with a width ~7 mm and is about 18% of the characteristic length of a specimen. Once the localized band formed, the strain concentrated in this area increases rapidly as the loading progresses (Figure 7(a)). Especially, the averaged strain component $\bar{\varepsilon}_Y$ perpendicular to the rupture surface in this localized band presents a sharp increase in the vicinity of rupture (Figure 7(a)). In order to characterize this accelerating behavior, based on equation (1), the response function corresponding to these zonal areas is defined as

$$R_z = \frac{w_z d\bar{\varepsilon}_Y}{dU} \tag{6}$$

where z denotes the concerned zone and w_z is the width of the zonal area. The linear part of the normalized zonal response function $R_z/R_{z,\mathrm{end}}$ with respect to $1 - U/U_{\mathrm{F}}$ in the double logarithmic

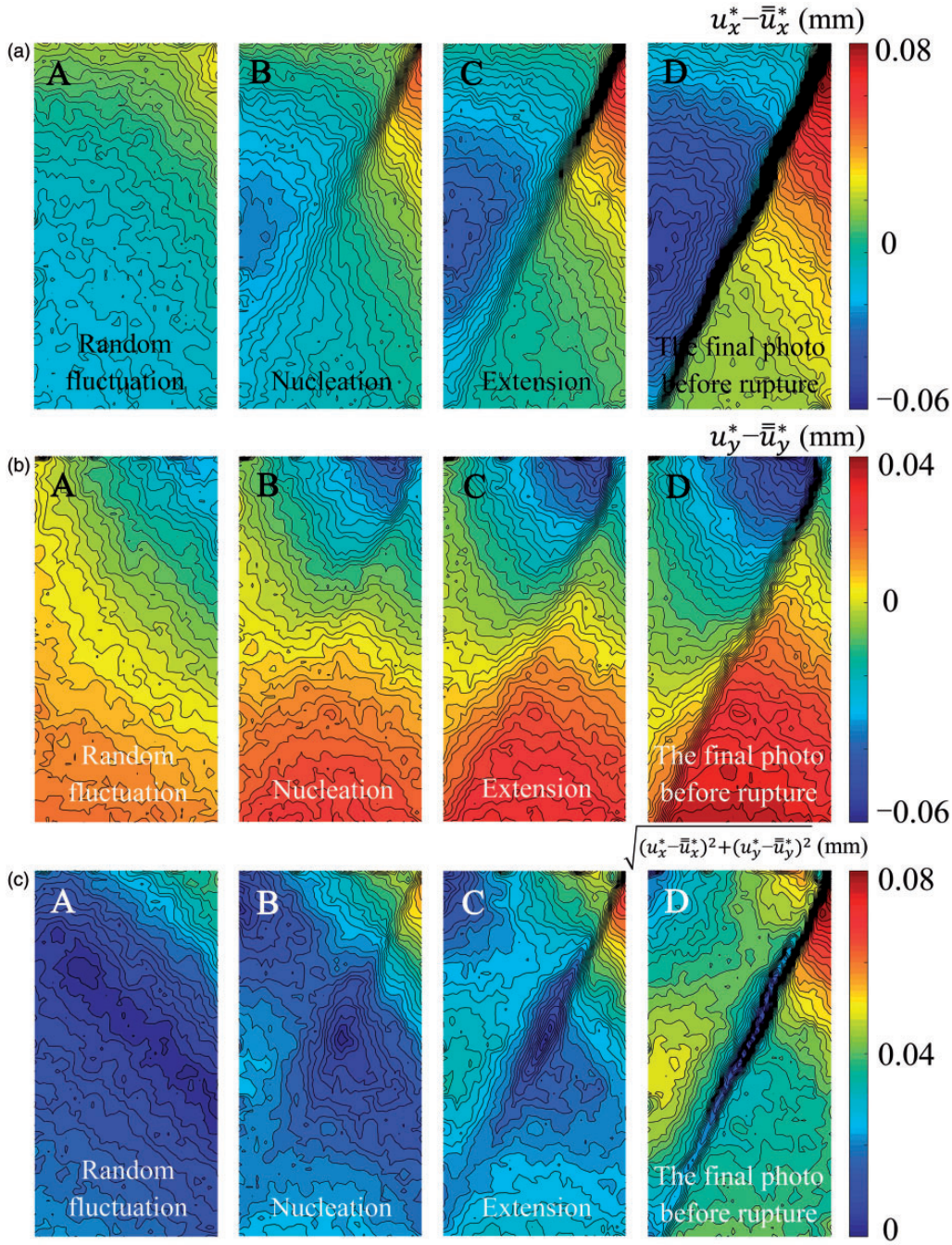

Figure 4. The evolution of the displacement field on the surface of a specimen. Here, the average values of displacement components of the entire field of the specimen, namely $\overline{\overline{u}}_x^*$ and $\overline{\overline{u}}_y^*$, have been removed. (a) The field of $u_x^* - \overline{\overline{u}}_x^*$. (b) The field of $u_y^* - \overline{\overline{u}}_y^*$. (c) The field of $\sqrt{(u_x^* - \overline{\overline{u}}_x^*)^2 + (u_y^* - \overline{\overline{u}}_y^*)^2}$. The letters A, B, C, and D in the figures correspond to the representative states illustrated in Figure 2, respectively.

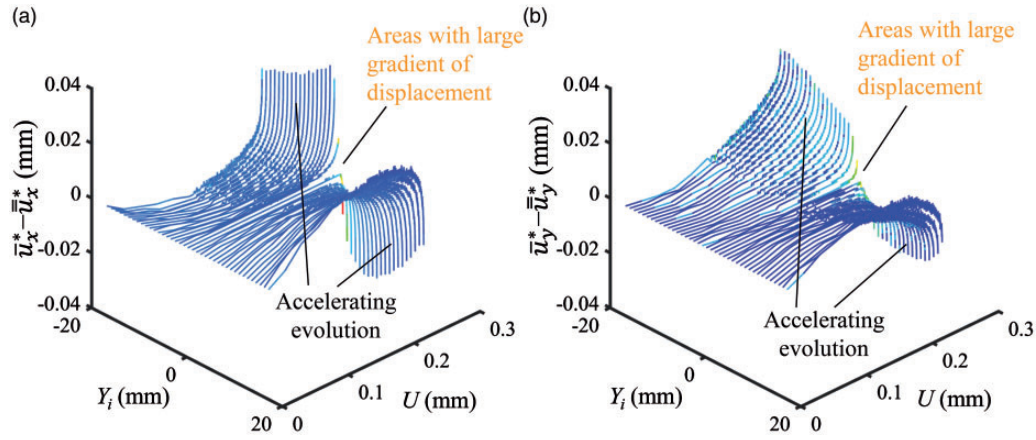

Figure 5. The spatio-temporal evolution of the average displacement of the zonal areas. Here, the average values of displacement components of the entire field of the specimen, namely $\bar{\bar{u}}_x^*$ and $\bar{\bar{u}}_y^*$, have been removed. (a) $\bar{u}_x^*(Y_i,U) - \bar{\bar{u}}_x^*(U)$ and (b) $\bar{u}_y^*(Y_i,U) - \bar{\bar{u}}_y^*(U)$ correspond to the spatio-temporal evolution of the average displacement components along *x*- and *y*-directions in a narrow zonal area located at Y_i. The highlighted part near the rupture surface ($Y = 0$ mm) indicates a large gradient of the displacement.

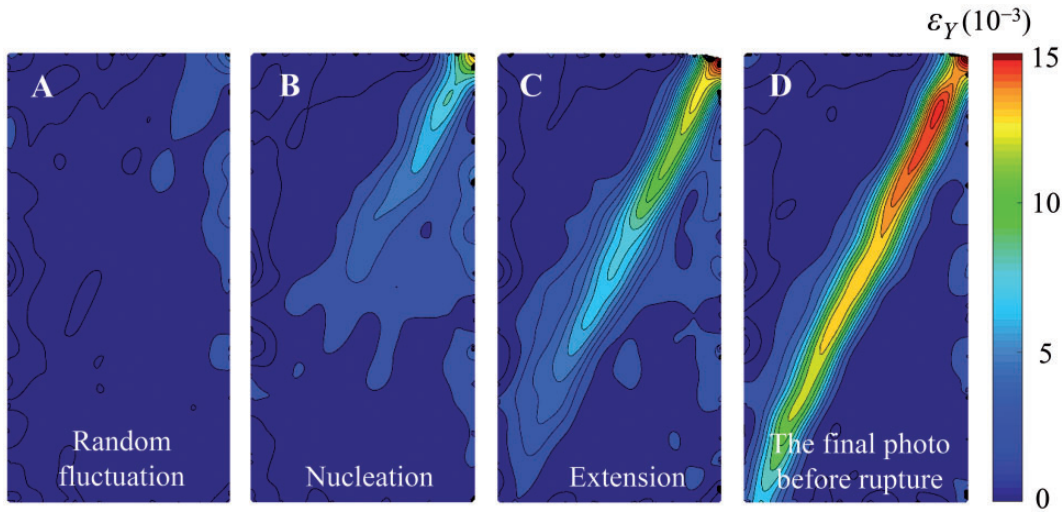

Figure 6. The evolution and localization of the vertical strain field on the surface of a specimen. Here ε_Y is the strain component perpendicular to the rupture surface. Four subgraphs A, B, C and D correspond to the representative states illustrated in Figure 2.

graph shown in Figure 7(b) indicates that the acceleration behavior of R_z follows a power-law relationship

$$R_z = B_{\mathrm{F},z}(1 - U/U_{\mathrm{F}})^{\beta_{\mathrm{F},z}} \tag{7}$$

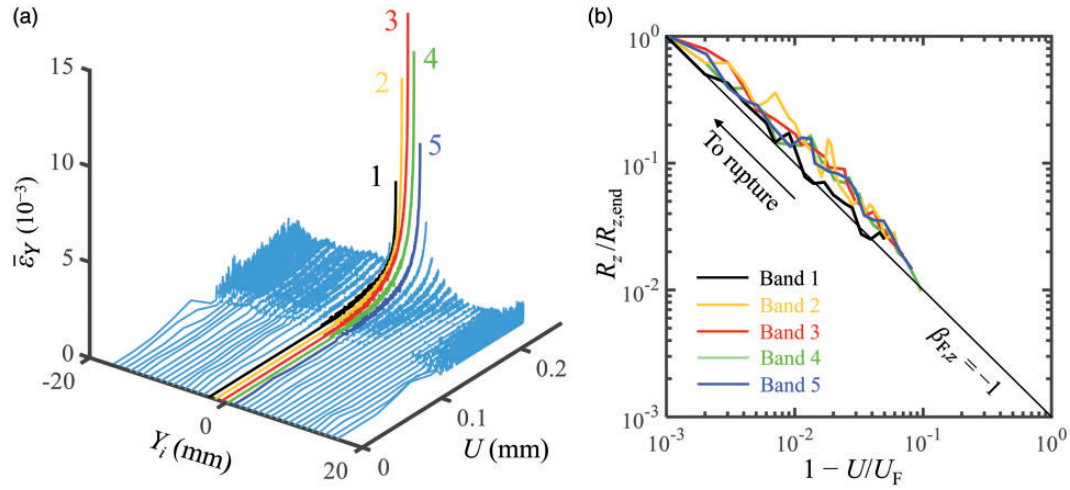

Figure 7. The emergence of the power-law singularity of the response function R_z in zonal areas near the rupture surface. (a) Accelerating evolution of the average strain component $\bar{\varepsilon}_Y$ perpendicular to the rupture surface in each zonal area and (b) the power-law singularity of the normalized zonal response function $R_z/R_{z,end}$, corresponding to the zones 1 to 5 with different distances to the rupture surface in (a). Here $R_{z,end}$ is the last value of R_z captured before rupture.

with U approaching to U_F, where $B_{F,z}$ is a parameter, $\beta_{F,z}$ is the power-law singularity exponent in the zonal area, and the normalization factor $R_{z,end}$ is set to be the last value of R_z captured before rupture, for the increase of R_z is monotonous and its last value is the maximum. When $U = U_F$, R_z will tend to infinite. The least square fitting shows that the power-law singularity exponent $\beta_{F,z}$ in all zonal areas in the localized band almost presents an identical value of $\beta_{F,z} = -1$ (Figure 7(b)).

Power-law singularity and localization are two essential characteristics of catastrophic rupture (Figure 8). The former shows the temporal acceleration evolution of the strain in the localized band, and the latter reflects the spatial accumulation of deformations and damages. The power-law acceleration coupled with localization of deformation and damage induces the eventual catastrophic rupture.

Trans-scale characteristic of power-law singularity

The coupled relationship between localization and power-law acceleration exhibits a trans-scale characteristic, which can be characterized by various response functions R_z in various sampling zones with a variable width w (see Figure 9(a)). The center of the sampling zone is set on the rupture surface, and the area of the sampling zone and the whole observed surface of a specimen are denoted as A_w and A_0, respectively. As A_w changes with w, R_z always presents the power-law singularity (Figure 9(a)), but the values of the power-law exponent $\beta_{F,z}$ increase with the increase of A_w (Figure 9(b)). When the sampling zone is narrow ($A_w/A_0 \to 0$) and covers the rupture surface where the strain is concentrated, $\beta_{F,z}$ is almost equal to -1. In contrast, when the sampling zone covers the whole observed specimen surface ($A_w/A_0 = 1$), R_z becomes the macroscopic average response of the whole specimen. Therefore, the global power-law singularity exhibited by the response function R (equation (5)) and others calculated in different sampling

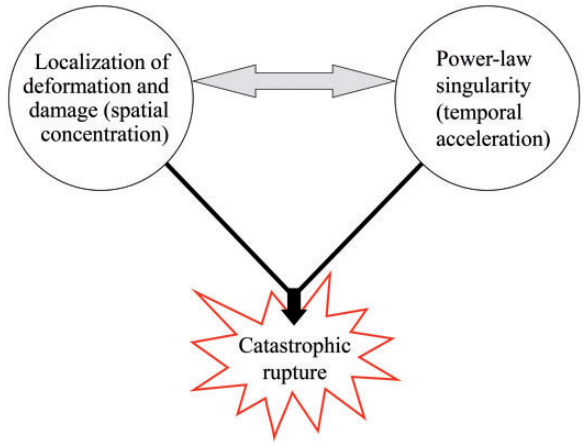

Figure 8. A sketched relationship between localization of deformation and damage, power-law singularity and eventual catastrophic rupture.

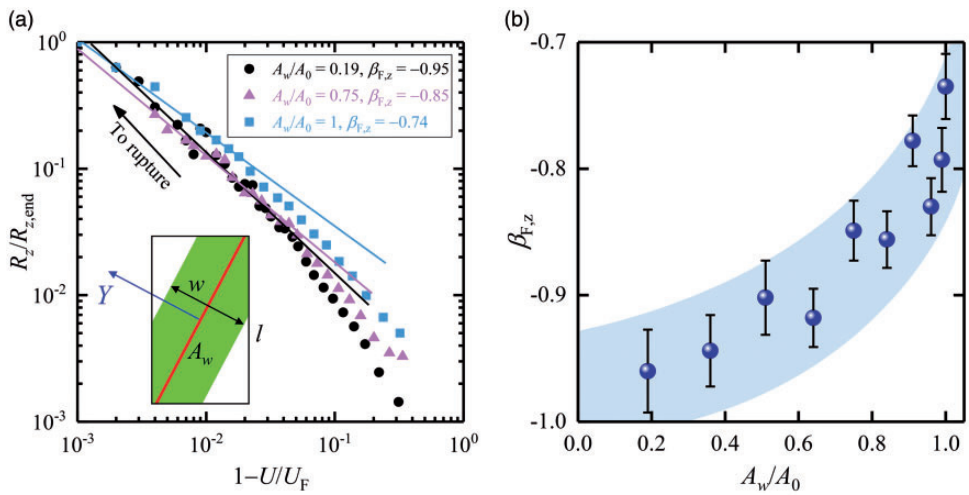

Figure 9. The trans-scale characteristics of the power-law singularity. (a) The log–log relation between the normalized responses function $R_z/R_{z,end}$ and the normalized governing displacement, showing the power-law behavior with different values of exponent resulting from the different widths of the sampling zones across the rupture surface. Here, as shown in the inset, w is the width of the sampling zone across the rupture surface and l is the characteristic length of the specimen. A_w and A_0 are the areas of the sampling zone and the whole observed surface of a specimen, respectively. (b) Power-law singularity exponent varies with the area of the sampling zone across the rupture surface.

zones all come from the singular response of the localized band. Furthermore, it has been demonstrated that the power-law exponent β_F of the global response function R inherently ranges from $-1/2$ to -1 (Xue et al., 2018). Therefore, the power-law exponent $\beta_{F,z}$ of R_z also falls into this range.

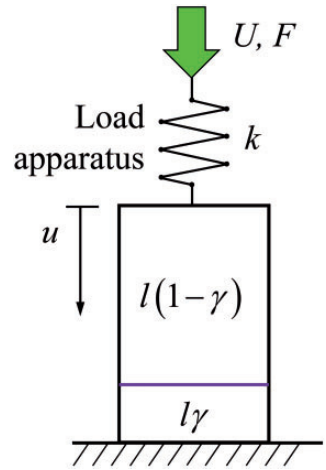

Figure 10. A simplified mean-field model for a series system consisting of a specimen with localized deformation band and the loading apparatus. Here l and γ represent the characteristic length of the specimen and the proportion of the localized band in the specimen, respectively. The spring with a stiffness k represents the load apparatus. u is the deformation of the specimen. U and F represent the governing displacement and force of the testing machine.

Analytical description of relationship between localization and power-law singularity

The trans-scale characteristic of the power-law singularity and its relationship with localization can be further demonstrated based on a simplified mean-field model (Hao et al., 2007, 2010). When localization occurs, a specimen can be regarded as two parts in series (Figure 10), i.e., a localized zone with continuing deformation and a non-localized zone (unloading zone) with potential release of elastic energy. The load apparatus remains the other elastic part with stiffness k. The relative scale of the localized band to the characteristic length l of a sample is γ. Then, the whole deformation of a specimen can be expressed as

$$u = u_{1-\gamma} + u_{\gamma} \tag{8}$$

where $u_{1-\gamma}$ and u_{γ} represent the deformations of the non-localized zone and the localized zone, respectively. Then the response function of a specimen $R = du/dU$ can be rewritten as

$$R = \frac{du_{1-\gamma}}{dU} + \frac{du_{\gamma}}{dU} \tag{9}$$

The deformation $u_{1-\gamma}$ of the non-localized zone is

$$u_{1-\gamma} = \varepsilon_{1-\gamma}(1-\gamma)l \tag{10}$$

where $\varepsilon_{1-\gamma}$ is the average strain of the non-localized zone. Therefore

$$du_{1-\gamma} = d\left[\varepsilon_{1-\gamma}(1-\gamma)l\right] = l\left[(1-\gamma)d\varepsilon_{1-\gamma} + \varepsilon_{1-\gamma}d(1-\gamma)\right] \tag{11}$$

In equation (11), $l(1-\gamma)$, $\varepsilon_{1-\gamma}$ and both of their increments are finite (see Figures 6, 7 and 10), so $du_{1-\gamma} < \infty$. Additionally, dU is also finite. Thus, in equation (9), $du_{1-\gamma}/\mathrm{d}U$ does not cause the singularity. Meanwhile, the deformation of localized zone is

$$u_\gamma = \int_0^{l\gamma(U)} \varepsilon_\gamma(y, U)\mathrm{d}y \tag{12}$$

where ε_γ is the average strain of the localized zone. Then

$$\frac{du_\gamma}{dU} = \int_0^{l\gamma(U)} \frac{d\varepsilon_\gamma(y, U)}{dU}\mathrm{d}y + \varepsilon_\gamma(\gamma l, U)\frac{ld\gamma}{dU} \tag{13}$$

In equation (13), ε_γ, $l\gamma$, and $\mathrm{d}\gamma/\mathrm{d}U$ are finite, thus the second term to the right of equation (13) does not tend to singularity. Moreover

$$\bar{\varepsilon}_\gamma = \frac{1}{l\gamma}\int_0^{l\gamma(U)} \varepsilon_\gamma(y, U)\mathrm{d}y \tag{14}$$

leads to that

$$R_z = \frac{l\gamma d\bar{\varepsilon}_\gamma}{dU} = \int_0^{l\gamma(U)} \frac{d\varepsilon_\gamma(y, U)}{dU}\mathrm{d}y \tag{15}$$

Consequently, the singularity of the global response function R (equation (9)) results from the singularity of the response function R_z (equation (15)) in the localized band.

Predicting catastrophic rupture based on power-law singularity of localized band

The power-law singularity of localized band gives a way to predict catastrophic rupture through the evolving process of the local information. For the sake of prediction, equation (7) is rewritten as a linear form that

$$R_z^{1/\beta_{\mathrm{F},z}} = C(U_\mathrm{F} - U) \tag{16}$$

where $C = B_{\mathrm{F},z}^{1/\beta_{\mathrm{F},z}}/U_\mathrm{F}$. When $U = U_\mathrm{F}$, $R_z^{1/\beta_{\mathrm{F},z}} = 0$. Hence, U_F can be determined by linearly extrapolating the line $R_z^{1/\beta_{\mathrm{F},z}}$ to the abscissa. This kind of prediction method has been validated and applied in many catastrophic ruptures and natural hazards especially when $\beta_{\mathrm{F},z} = -1$ (Cornelius and Voight, 1994, 1995; Kilburn, 2003; Kilburn and Voight, 1998; Voight, 1988). However, because of the trans-scale characteristic of the power-law singularity mentioned above and the inherent changeability (Xue et al., 2018), the power-law exponent is not always equal to -1. Moreover, the value of $\beta_{\mathrm{F},z}$ is even unknown before rupture. To solve this problem for prediction, Xue et al. (2018) suggest a prediction method by replacing U_F with the current sampling endpoint U_t in equation (7), and then the response function in a zonal area can be expressed as

$$R_z = B_{t,z}(1 - U/U_t)^{\beta_{t,z}} \tag{17}$$

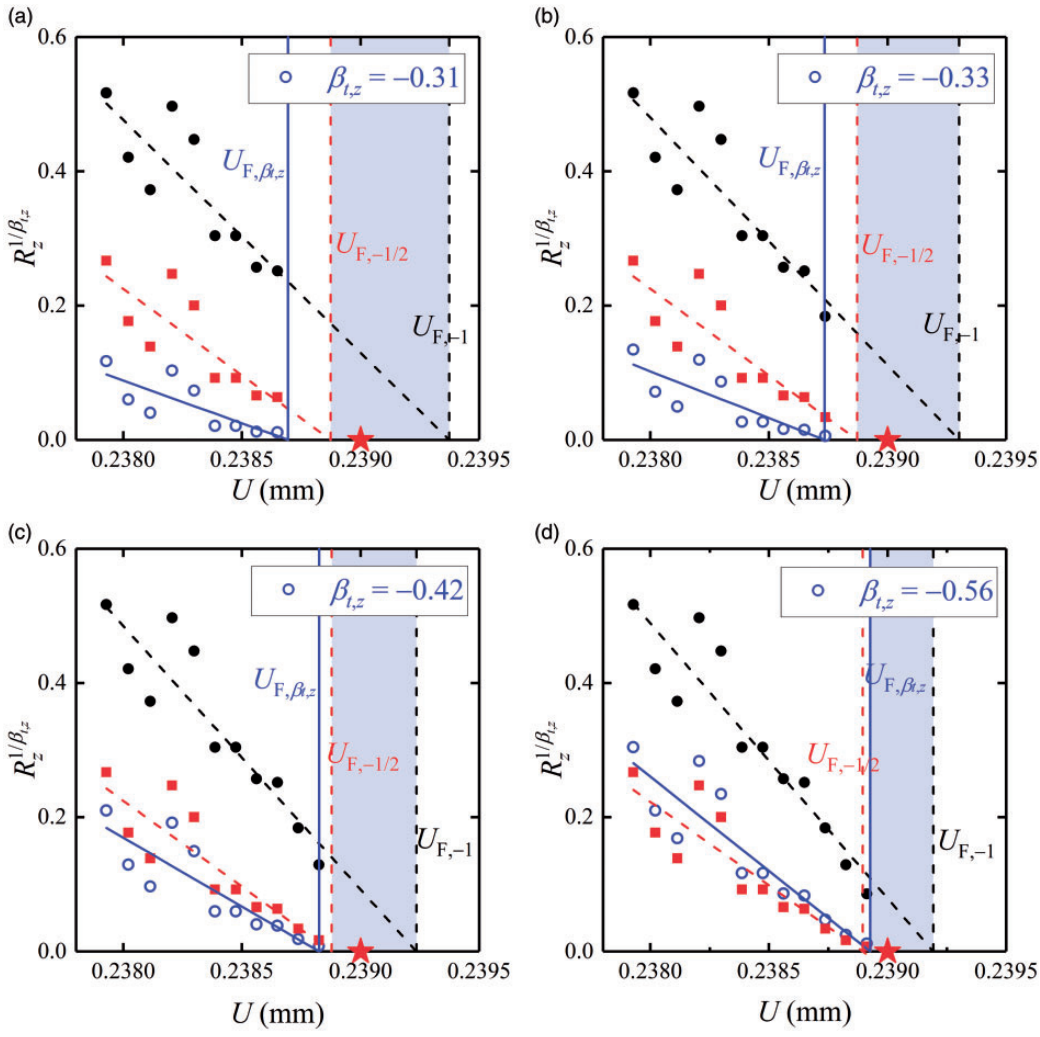

Figure 11. A prediction of the catastrophic rupture based on the zonal response function and the range of the power-law exponent from −1 to −1/2. Here, as an example, the zonal response function is adopted from the zone 3 in Figure 7. The red pentagram denotes the rupture point, i.e., $U_F = 0.2390$ mm. Both $U_{F,\beta t,z}$ and $U_{F,-1/2}$ provide the predicted lower bounds of the catastrophic rupture, and $U_{F,-1}$ is the upper bound, respectively. (a) $\beta_{t,z} = -0.31$, $U_{F,\beta t,z} = 0.2386$ mm, $U_{F,-1/2} = 0.2389$ mm, $U_{F,-1} = 0.2394$ mm. (b) $\beta_{t,z} = -0.33$, $U_{F,\beta t,z} = 0.2387$ mm, $U_{F,-1/2} = 0.2389$ mm, $U_{F,-1} = 0.2393$ mm. (c) $\beta_{t,z} = -0.42$, $U_{F,\beta t,z} = 0.2388$ mm, $U_{F,-1/2} = 0.2389$ mm, $U_{F,-1} = 0.2392$ mm. (d) $\beta_{t,z} = -0.56$, $U_{F,\beta t,z} = 0.2389$ mm, $U_{F,-1/2} = 0.2389$ mm, $U_{F,-1} = 0.2392$ mm.

where $B_{t,z}$ is a parameter and $\beta_{t,z}$ is the reduced exponent. Experimental results indicate that $\beta_{t,z}$ decreases as U_t approaches to U_F (Xue et al., 2018). Apparently, $\beta_{t,z} = \beta_{F,z}$ when $U_t = U_F$ (see equations (7) and (17)). Similarly, the linearizing form of equation (17) can be written as

$$R_z^{1/\beta_{t,z}} = C_t(U_t - U) \tag{18}$$

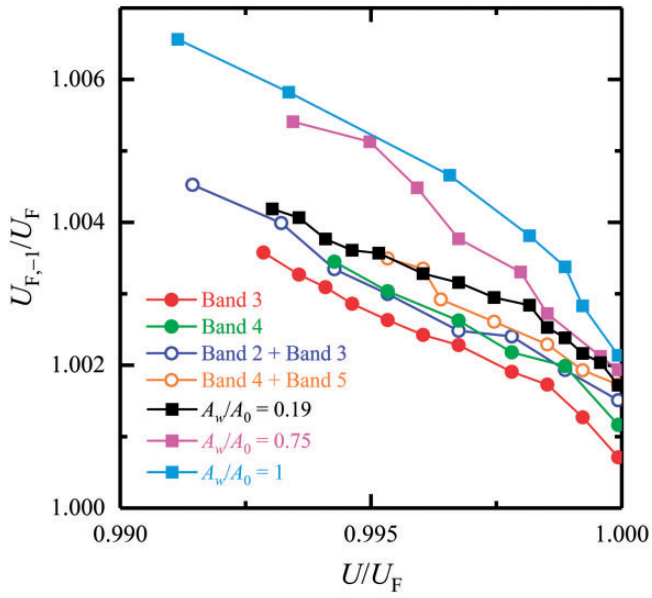

Figure 12. The comparison of predictions made by means of the zonal strain field information, but either from the narrow zones in the localized band with different distances to the rupture surface (circle) or from the zones with different areas across the rupture surface (square). A_w and A_0 are the areas of the sampling zone (Figure 9(a)) and the whole observed specimen surface, respectively.

where $C_t = B_{t,z}^{1/\beta_{t,z}}/U_t$. It is clear that $R_z^{1/\beta_{t,z}}$ has a linear relationship with U, and the intersection of $R_z^{1/\beta_{t,z}}$ and the abscissa will be the lower bound (denoted as $U_{F,\beta t,z}$) of U_F. Furthermore, as the analysis before, $\beta_{F,z}$ ranges from $-1/2$ to -1, and $\beta_{F,z}$ is the lower bound of $\beta_{t,z}$. Substituting $-1/2$ for $\beta_{t,z}$ in equation (18), the another lower bound (denoted as $U_{F,-1/2}$) of U_F can be predicted (Figure 11). Similarly, the upper bound (denoted as $U_{F,-1}$ in Figure 11) of U_F can be determined by setting $\beta_{t,z} = -1$. As an example, Figure 11 shows details of a predicting process based on the power-law acceleration behavior of response function of band 3 in Figure 7. It is seen that the prediction interval constructed by the lower and upper bounds containing U_F narrows gradually as sampling in real-time. Both predicted values of the lower and upper bounds consistently converge to the actual value U_F as U_t approaching to the real rupture point U_F.

Figure 12 illustrates the real-time prediction results of the upper bounds with different sizes of the sampling zone. It is shown that the power-law precursor of response function in different zonal areas with different sizes of the sampling zone gives good predictions, although it has different values of the power-law exponent. This implies that the local information monitored at the stations in the zonal areas may be available to predict the occurrence time of catastrophic rupture in spite of the existence of localization. And the narrower is the sampling zone surrounding the rupture surface, the predicted values is closer to U_F. These results provide an operability and a convenience in application, since it is no longer necessary to capture the complete spatiotemporal information of the whole field in practice at all.

Conclusions

In summary, the present study reveals a close relationship between the localization of deformation and the power-law singularity, both characterizing the catastrophic rupture. It is found that the

accelerating evolution of the strain in the zones near or across the rupture surface always exhibits a power-law singularity, but with a changeable power-law exponent from $-1/2$ to -1, prior to catastrophic rupture. In particular, as the concerned zone, either near or across the rupture surface, gets closer to the rupture surface or narrower, the power-law singularity exponent decreases, nearly down to -1, showing a location-dependent characteristic. This power-law singularity obtained in these zonal areas can be used to make prediction of the occurrence time of catastrophic rupture in real-time. Furthermore, owing to the scale-invariance of power-law, the reported results imply a feasibility to predict the catastrophic rupture in even larger scales, perhaps earthquakes based on the surveys in the local areas nearby the faults.

Declaration of conflicting interests

The author(s) declared no potential conflicts of interest with respect to the research, authorship, and/or publication of this article.

Funding

The author(s) disclosed receipt of the following financial support for the research, authorship, and/or publication of this article: This work is supported by the Strategic Priority Research Program (B) of the Chinese Academy of Sciences (XDB22040501), and the National Natural Science Foundation of China (grants 11432014 and 11672258).

ORCID iD

Jian Xue https://orcid.org/0000-0003-0627-4136

References

Bai Y, Xia M, Ke F, et al. (2001) Statistical microdamage mechanics and damage field evolution. *Theoretical and Applied Fracture Mechanics* 37: 1–10.

Baud P, Klein E and Wong T (2004) Compaction localization in porous sandstones: Spatial evolution of damage and acoustic emission activity. *Journal of Structural Geology* 26: 603–624.

Ben-Zion Y and Lyakhovsky V (2002) Accelerated seismic release and related aspects of seismicity patterns on earthquake faults. *Pure and Applied Geophysics* 10: 2385–2412.

Boué A, Lesage P, Cortés G, et al. (2015) Real-time eruption forecasting using the material Failure Forecast Method with a Bayesian approach. *Journal of Geophysical Research* 120: 2143–2161.

Colpo AB, Kosteski LE and Iturrioz I (2017) The size effect in quasi-brittle materials: Experimental and numerical analysis. *International Journal of Damage Mechanics* 26: 395–416.

Cook NGW (1965) The failure of rock. *International Journal of Rock Mechanics and Mining Sciences & Geomechanics Abstracts* 2: 389–403.

Cornelius RR and Scott P (1993) A materials failure relation of accelerating creep as empirical description of damage accumulation. *Rock Mechanics and Rock Engineering* 26: 233–252.

Cornelius RR and Voight B (1994) Seismological aspects of the 1989–1990 eruption at Redoubt Volcano, Alaska: The Materials Failure Forecast Method (FFM) with RSAM and SSAM seismic data. *Journal of Volcanology and Geothermal Research* 62: 469–498.

Cornelius RR and Voight B (1995) Graphical and PC-software analysis of volcano eruption precursors according to the materials failure forecast method (FFM). *Journal of Volcanology and Geothermal Research* 64: 295–320.

Dewers TA, Issen KA, Holcomb DJ, et al. (2017) Strain localization and elastic-plastic coupling during deformation of porous sandstone. *International Journal of Rock Mechanics and Mining Sciences* 98: 167–180.

Hao S, Liu C, Lu C, et al. (2016) A relation to predict the failure of materials and potential application to volcanic eruptions and landslides. *Scientific Reports* 6: 27877.

Hao S, Rong F, Lu M, et al. (2013) Power-law singularity as a possible catastrophe warning observed in rock experiments. *International Journal of Rock Mechanics and Mining Sciences* 60: 253–262.

Hao S, Wang H, Xia M, et al. (2007) Relationship between strain localization and catastrophic rupture. *Theoretical and Applied Fracture Mechanics* 48: 41–49.

Hao S, Xia M, Ke F, et al. (2010) Evolution of localized damage zone in heterogeneous media. *International Journal of Damage Mechanics* 19: 787–804.

Hao S, Yang H and Elsworth D (2017) An accelerating precursor to predict ''time-to-failure'' in creep and volcanic eruptions. *Journal of Volcanology and Geothermal Research* 343: 252–262.

Harnett CE, Benson PM, Rowley P, et al. (2018) Fracture and damage localization in volcanic edifice rocks from El Hierro, Stromboli and Tenerife. *Scientific Reports* 8: 1942.

Helmstetter A, Sornette D, Grasso J-R, et al. (2004) Slider-block friction model for landslides: Application to Vaiont and La Clapière landslides. *Journal of Geophysical Research* 109: B02409.

Hill R and Hutchinson JW (1975) Bifurcation phenomena in the plane tension test. *Journal of the Mechanics and Physics of Solids* 23: 239–264.

Jin L, Ding Z, Li D, et al. (2018) Experimental and numerical investigations on the size effect of moderate high-strength reinforced concrete columns under small-eccentric compression. *International Journal of Damage Mechanics* 27: 657–685.

Jin Y, Xia M and Wang H (2012) Uncertainty and universality in the power-law singularity as a precursor of catastrophic rupture. *Science China Physics, Mechanics and Astronomy* 55: 1098–1102.

Kale S and Ostoja-Starzewski M (2017) Representing stochastic damage evolution in disordered media as a jump Markov process using the fiber bundle model. *International Journal of Damage Mechanics* 26: 147–161.

Kilburn CRJ (2003) Multiscale fracturing as a key to forecasting volcanic eruptions. *Journal of Volcanology and Geothermal Research* 125: 271–289.

Kilburn CRJ (2012) Precursory deformation and fracture before brittle rock failure and potential application to volcanic unrest. *Journal of Geophysical Research* 117: B02211.

Kilburn CRJ and Voight B (1998) Slow rock fracture as eruption precursor at Soufriere Hills Volcano, Montserrat. *Geophysical Research Letters* 25: 3665–3668.

Li H, Bai Y, Xia M, et al. (2000) Damage localization as a possible precursor of earthquake rupture. *Pure and Applied Geophysics* 157: 1929–1943.

Li W and Wu J (2018) A consistent and efficient localized damage model for concrete. *International Journal of Damage Mechanics* 27: 541–567.

Lockner DA, Byerlee JD, Kuksenko V, et al. (1991) Quasi-static fault growth and shear fracture energy in granite. *Nature* 350: 39–42.

Main IG (1999) Applicability of time-to-failure analysis to accelerated strain before earthquakes and volcanic eruptions. *Geophysical Journal International* 139: F1–F6.

Main IG, Sammonds PR and Meredith PG (2010) Application of a modified Griffith criterion to the evolution of fractal damage during compressional rock failure. *Geophysical Journal of the Royal Astronomical Society* 115: 367–380.

Markeset G and Hillerborg A (1995) Softening of concrete in compression – Localization and size effects. *Cement and Concrete Research* 25: 702–708.

Rong F, Wang H, Xia M, et al. (2006) Catastrophic rupture induced damage coalescence in heterogeneous brittle media. *Pure and Applied Geophysics* 163: 1847–1865.

Rudnicki JW and Rice JR (1975) Conditions for the localization of deformation in pressure-sensitive dilatant materials. *Journal of the Mechanics and Physics of Solids* 23: 371–394.

Salamon MDG (1970) Stability, instability and design of pillar workings. *International Journal of Rock Mechanics and Mining Sciences & Geomechanics Abstracts* 7: 613–631.

Smith R and Kilburn CRJ (2010) Forecasting eruptions after long repose intervals from accelerating rates of rock fracture: The June 1991 eruption of Mount Pinatubo, Philippines. *Journal of Volcanology and Geothermal Research* 191: 129–136.

Sornette D and Sammis CG (1995) Complex critical exponents from renormalization group theory of earthquakes: Implications for earthquake predictions. *Journal De Physique I* 5: 607–619.
Toussaint R and Pride SR (2002) Fracture of disordered solids in compression as a critical phenomenon. III. Analysis of the localization transition. *Physical Review E* 66: 036137.
Voight B (1988) A method for prediction of volcanic eruptions. *Nature* 332: 125–130.
Voight B (1989) A relation to describe rate-dependent material failure. *Science* 243: 200–203.
Voight B and Cornelius RR (1991) Prospects for eruption prediction in near real-time. *Nature* 350: 695–698.
Wei Y, Xia M, Ke F, et al. (2000) Evolution-induced catastrophe and its predictability. *Pure and Applied Geophysics* 157: 1945–1957.
Xu X, Ma S, Xia M, et al. (2004) Damage evaluation and damage localization of rock. *Theoretical and Applied Fracture Mechanics* 42: 131–138.
Xue J, Hao S, Wang J, et al. (2018) The changeable power law singularity and its application to prediction of catastrophic rupture in uniaxial compressive tests of geomedia. *Journal of Geophysical Research* 123: 2645–2657.

Appendix

Notation

A_{w}	the area of the sampling zone on a specimen surface
A_0	the area of the observed surface of a specimen
l	characteristic length of a specimen
R	response function of a specimen, $R = du/dU$
R_{z}	response function in a zonal area, $R_z = \frac{w_z d\bar{\varepsilon}_Y}{dU}$, where z denotes the concerned zone, while w_z and $\bar{\varepsilon}_Y$ are the width and the average strain in the concerned zone, respectively
u	deformation of a whole specimen along loading direction
u_x^*, u_y^*	components of the displacement field along x- and y-direction on the observed surface of a specimen
$\bar{u}_x^*$, $\bar{u}_y^*$	average values of u_x^* and u_y^* in a zonal area on the observed surface of a specimen
$\overline{\overline{u}}_x^*$, $\overline{\overline{u}}_y^*$	components of the global average displacement on the observed surface of a specimen
U	governing displacement of the testing machine
U_{F}	displacement of the testing machine at catastrophic rupture
$U_{\mathrm{F},\beta t,z}$	lower bound of U_{F} predicted by using $\beta_{t,z}$
$U_{\mathrm{F},-1/2}$	lower bound of U_{F} predicted by using $\beta_{t,z} = -1/2$
$U_{\mathrm{F},-1}$	upper bound of U_{F} predicted by using $\beta_{t,z} = -1$
U_t	governing displacement of the testing machine at real-time termination of data sampling
w	the width of the sampling zone on a specimen surface
w_{z}	the width of the zonal area
β_{F}	power-law exponent of R
$\beta_{\mathrm{F},z}$	power-law exponent of R_z
$\beta_{t,z}$	reduced exponent of R_z
γ	the ratio of the width of the localized band to the characteristic length of a specimen
ε_Y	strain component perpendicular to the rupture surface
$\bar{\varepsilon}_Y$	average value of ε_Y in a zonal area on the observed surface of a specimen